Chinese Journal of
POLYMER SCIENCE

RESEARCH ARTICLE

https://doi.org/10.1007/s10118-022-2775-4
Chinese J. Polym. Sci. **2023**, *41*, 525–537

Tumor-Penetrating and Mitochondria-Targeted Drug Delivery Overcomes Doxorubicin Resistance in Lung Cancer

Meng-Xue Zhou[a,b,†], Jia-Yu Zhang[a,†], Xiao-Meng Cai[a,†], Rui Dou[a], Li-Fo Ruan[a], Wen-Jiang Yang[c], Wen-Chu Lin[d], Jun Chen[a*], and Yi Hu[a*]

[a] *CAS Key Laboratory for Biomedical Effects of Nanomaterials and Nanosafety, Institute of High Energy Physics and University of Chinese Academy of Sciences (UCAS), Chinese Academy of Sciences (CAS), Beijing 100049, China*
[b] *Key Laboratory of Tea Biology and Resource Utilization of Ministry of Agriculture, Tea Research Institute, Chinese Academy of Agricultural Sciences, Hangzhou 310008, China*
[c] *Division of Nuclear Technology and Applications, Institute of High Energy Physics, Chinese Academy of Sciences (CAS), Beijing 100049, China*
[d] *High Magnetic Field Laboratory, Hefei Institutes of Physical Science, Chinese Academy of Sciences, Hefei 230031, China, University of Science and Technology of China, Hefei 230026, China*

Electronic Supplementary Information

Abstract As one of the major challenges in tumor chemotherapy, multidrug resistance typically correlates with the poor drug penetration within tumor tissues and drug efflux by the ATP-driven efflux pumps in tumor cells. Herein, we design a kind of near-infrared (NIR) light- and acidity-activated micellar iPUTDN nanoparticle for mitochondria-targeting doxorubicin (DOX) delivery to combat DOX resistance in small-cell lung cancer. While the PEGylated iPUTDN nanoparticles can keep stealth in blood circulation, NIR irradiation at the tumor region can peel off the PEG shell from the nanoparticles, and the exposed iRGD can facilitate deep tumor penetration of the nanoparticles. After being internalized by DOX-resistant H69AR cells, the poly(*β*-aminoester)s (PAE)-based nanoparticles can release the triphenylphosphonium (TPP)-conjugated DOX (TDOX) into the cytosol, which can further accumulate in mitochondria with the aid of TPP. Consequently, the mitochondrial membrane potential and ATP content are both reduced in DOX-resistant H69AR cells. The *in vivo* therapeutic results show that TDOX-loaded nanoparticles with the aid of NIR light irradiation can effectively suppress the DOX-resistant small-cell lung cancer without noticeable adverse effects.

Keywords Doxorubicin; NIR/pH-dual sensitive nanoparticles; Tumor penetration; Mitochondria; Drug resistance

Citation: Zhou, M. X.; Zhang, J. Y.; Cai, X. M.; Dou, R.; Ruan, L. F.; Yang, W. J.; Lin, W. C.; Chen, J.; Hu, Y. Tumor-penetrating and mitochondria-targeted drug delivery overcomes doxorubicin resistance in lung cancer. *Chinese J. Polym. Sci.* **2023**, *41*, 525–537.

INTRODUCTION

The occurrence of multidrug resistance compromises the effectiveness of tumor chemotherapy.[1–3] The superfamily of ATP-binding cassette (ABC) transporter in drug-resistant cells, such as P-glycoprotein (Pgp), plays a pivotal role in multidrug resistance, recognizing and promoting the efflux of drugs from cancer cells in an ATP-driven way.[4,5] Therefore, dwindling ATP production may effectively suppress the function of ABC transporters,[6,7] which could be achieved by impairing mitochondria where ATP is synthesized.[8] However, current first-line anticancer drugs are incapable of directly suppressing mitochondrial function of energy supply to overcome drug resistance.

Accumulation evidence from our group and others suggests that targeted delivery of drugs to mitochondria is a promising strategy to combat the drug resistance in tumor cells.[9–12] As a broad-spectrum anticancer drug, DOX has been extensively used for cancer chemotherapy.[13] Initially, researchers employ DOX or analogs merely to engage in damaging mitochondrial DNA, leading to a significantly enhanced cytotoxic effect in cancer cells.[14,15] Afterward, further studies unravel a new and potent function of mitochondria-targeted DOX in provoking a severe dysfunction of mitochondria due to the transition of DOX to semiquinone radicals for oxidative damage of membrane lipids, membrane-bound proteins, and enzymes in mitochondria.[16] Therefore, mitochondria-targeted delivery of DOX may directly interfere with the mitochondrial functions to combat drug resistance in a synergized action fashion.

The mitochondria-targeted delivery of DOX thus becomes a vital yet challenging step.[17–20] Free DOX possesses low mitochondria targeting. Improving the mitochondria-targeted delivery of DOX exploits conjugating mitochondrial targeting ligand onto DOX or engineering mitochondrial targeting nanocarriers.[13] Triphenylphosphonium (TPP), a highly posi-

* Corresponding authors, E-mail: chenjun@ihep.ac.cn (J.C.)
E-mail: huyi@ihep.ac.cn (Y.H.)
† These authors contributed equally to this work.
Special Issue: The Youth Innovation Promotion Association of the Chinese Academy of Sciences
Received April 7, 2022; Accepted April 25, 2022; Published online July 21, 2022

tive lipophilic cation, is an efficacious mitochondrial targeting ligand.[21,22] TPP-conjugated DOX (TDOX) has evidenced its high mitochondria-targeting efficacy *in vitro*.[23–25] However, the delivery efficiency of TDOX *in vivo* is limited by various physiological and pathological barriers, such as blood circulation, tumoral blood vessels, and heterogeneity of tumor stroma.[26] The nanoplatform with the rational integration of multiple stimuli-responsive properties is a promising tool to bypass those barriers.[27–30] Among them, the physicochemical change of nanoparticles through responsively peeling off PEGs under various signals facilitates them overcoming multiple barriers *in vivo*,[31] such as enhanced accumulation in tumors, improved tumor penetration, or increased cellular uptake.[32,33]

Herein, we develop a NIR light and tumor-acidity activated micellar nanoplatform, iPUTDN, for mitochondrial-targeted delivery of DOX to improve treatment against DOX resistant cancer. As outlined in Scheme 1, iPUTDN can maintain stealth in the circulation due to the PEG layer in nanoparticles afforded by the light-sensitive amphiphilic copolymers (PEG-Nbz-PAE-Nbz-PEG, HTMP). After accumulating in tumor tissues, the embedded UCNPs can convert *in situ* illuminated NIR light to UV light to cleave the Nbz bonds of HTMP in activating dePEGylation. As a result, iRGD groups in the amphiphilic copolymers (iRGD-PAE-iRGD, iPHT) are exposed to facilitate the intratumoral penetration and tumor cell uptake of nanoparticles. After endocytosis, the rapid protonation of PAE polymers in iPUTDN occurring in the lysosomal acidic milieu leads to rapid liberation of particles from lysosomes and a significantly elevated concentration of TDOX in the cytoplasm. The ultimate accumulation of TDOX at mitochondria induces mitochondrial dysfunctions to suppress the energy supply for Pgp-related bioactivities. In light of enhanced DOX accumulation in tumors and increased intracellular DOX levels, the present nanoplatform can effectively overcome drug resistance in H69AR cells.

EXPERIMENTAL

Materials

$NaYF_4$:Yb/Tm up-conversion nanoparticles (UCNPs) were purchased from Hefei Fluonano Biotech Co., Ltd. Anhydrous acetic acid, dimethyl sulfoxide (DMSO), chloroform, ethanol and cyclohexane were purchased from Beijing Chemical Reagent Company. Alfa Aesar Ltd. supplied *N*,*N*′-dicyclohexylcarbodiimide (DCC), 4,4′-trimethylene dipiperidine and 1,6-hexanediol diacrylate. JenKem Technology USA Inc. provided methoxy PEG amine (5K). iRGD (CRGDKGPDC) was purchased from GL Biochem (Shanghai) Ltd. Doxorubicin hydrochloride (DOX, 99.9%) was purchased from Adamas-beta. Aldrich Chemical Reagent Company provided sodium hydroxide (NaOH, 98%), sodium phosphate dibasic dodecahydrate, potassium phosphate monobasic, sodium chloride, potassium chloride, anhydrous sodium acetate and (4-carboxybutyl)triphenyl phosphonium bromide. *N*-hydroxysuccinimide (NHS) was purchased from Aladdin Chemical Co. DOX-resistant small-cell lung cancer cell line H69AR was kindly provided by Prof. Linglang Guo (Zhujiang Hospital, Southern Medical University). Fetal bovine serum (FBS) was purchased from PAN^{TM} Biotech, Germany. HyClone^{TM} offered 0.25% Trypsin-EDTA (1X) with

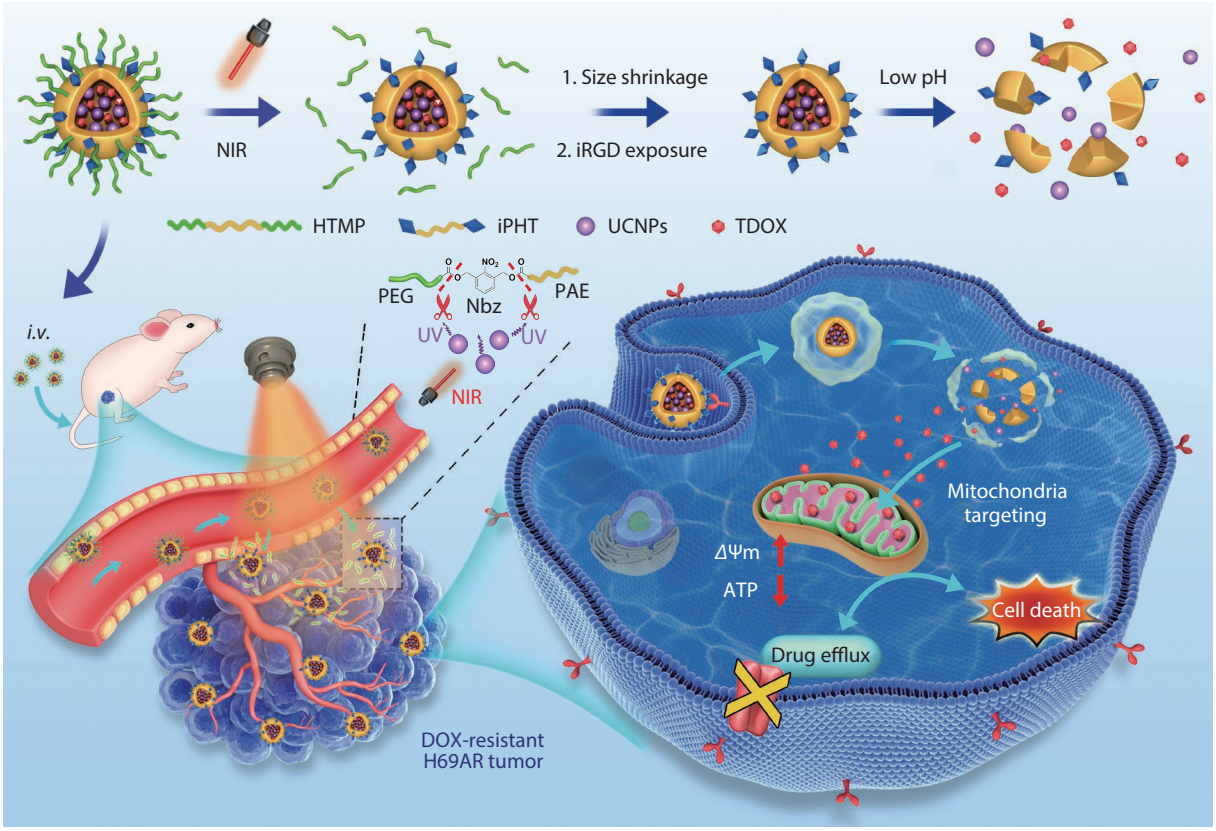

Scheme 1 Schematic illustration of mitochondria-targeted delivery based on iPUTDN and their effects in drug-resistant cancer cells.

https://doi.org/10.1007/s10118-022-2775-4

phenol red, Roswell Park Memorial Institute (RPMI) 1640 cell-culture medium and antibiotics (penicillin 100 U/mL and streptomycin 100 μg/mL). Beyotime Institute of Biotechnology (Shanghai, China) supplied ATP assay kit and JC-1 mitochondrial membrane potential assay kit. Dojindo Molecular Technologies (Kumamoto Techno, Japan) offered CCK-8 kit. Mitotracker and Hoechst 33342 were purchased from Life Technologies (Shanghai, China). Lumiprobe Corporation (USA) supplied Cy5 NHS ester. Heparin sodium salt was supplied from J&K Scientific Ltd (Beijing, China). Chloral hydrate (98.5%) was purchased from Acros Organics, ThermoFisher Scientific (China) Co., Ltd. Anti-CD31 antibody (ab28364) and Goat Anti-Rabbit IgG H&L (Alexa Fluor® 488) (ab150077) secondary antibody were purchased from Abcam. All of the chemicals were analytical grade and applied with no further purification. The experiments adopted deionized water.

Instruments

The collection of UV-Vis spectra was performed on a Varian Cary-50 UV-Vis spectrophotometer. The recording of fluorescence emission spectra was conducted on a Varian Cary Eclipse Fluorescence spectrophotometer. Up-conversion photoluminescence measurements were conducted on a PTI Quantamaster spectrofluorometer. A transmission electron microscope (TEM, Tecnai G2 20 S-TWIN, USA) was adopted to acquire morphologies of the samples. Zetasizer Nano ZS90 (Malvern Instruments Company, UK) was employed to perform dynamic light scatting (DLS) and zeta potential analysis. The Fourier transform Bruker EQUINOX55 spectrometer with the KBr pellet technique was employed to collect the Fourier transform infrared (FTIR) spectra. Confocal fluorescence microscopy (A1/LSM-Kit, Nikon) was employed to image the cells. The fluorescent images of mice were taken by PerkinElmer IVIS Lumina LT Series II Spectrum.

Synthesis and Characterization of HTMP and iPHT

The light-cleavage polymer (HTMP) and iRGD-containing polymer (iPHT) were synthesized according to a reported protocol with minor modifications.[30] Briefly, HTMP was synthesized *via* a Michael addition polymerization of 1,6-hexanediol diacrylate and 1.2-fold equivalent 4,4′-trimethylene dipiperidine, followed by two-stepped end-capping reactions of NPBMDA and methoxy PEG amine sequentially. Similarly, iPHT was synthesized *via* a Michael addition polymerization of 1,6-hexanediol diacrylate and 1.2-fold equivalent 4,4′-trimethylene dipiperidine, followed by an end-capping with iRGD peptide. Precipitation in a large amount of ether was adopted to purify the products, which was followed by drying in a vacuum. The chemical structure of obtained HTMP polymer was characterized by ^{1}H-NMR. ^{1}H-NMR ($CDCl_3$, δ, ppm): 1.20–1.50 (12H, —$(HCH)_2CH(CH_2)_3CH(HCH)_2$—, and 4H, —$CH_2CH_2$—), 1.60–1.75 (4H, —$(HCH)_2CH(CH_2)_3CH(HCH)_2$—, and 4H, —$CH_2CH_2OCO$—), 1.80–2.10 (4H, —$N(HCH)_2$—), 2.50–2.90 (4H, —$CH_2COO$—, and 4H, —$N(HCH)_2$—), 3.00–3.20 (4H, —$CH_2N(CH_2)_2$—), 3.40 (3H, —$OCH_3$), 3.50–3.80 ($CH_2$ in PEG repeat units), 4.10–4.30 (4H, —$COOCH_2$—), 5.25 (4H, —O—CH_2-bezene), 7.55 (3H, CH in benzene).

Preparation of iPHM Micelles and NIR Light-Sensitive iPHM@UCNPs (iPUN) Nanoparticles

The polymer micelle (iPHM) containing HTMP and iPHT was prepared by using the solvent substitution method. Typically, HTMP (10 mg) and iPHT (4 mg) were added and dissolved in 2 mL of DMF (the amount of substance ratio of HTMP/iPHM was 1). Then, 10 mL of distilled water was added dropwise under vigorously stirring. The solution was then moved to a dialysis bag and underwent extensive dialysis against PBS buffer (pH=7.4) to form micellar nanoparticles. iPUN composited nanoparticles were synthesized as follows: the dispersion of oleic acid-altered UCNPs was performed in cyclohexane at 10 mg/mL, followed by 15-min ultrasonic dispersion. HTMP (10 mg) and iPHT (4 mg) were dispersed in 1 mL of chloroform, then, 500 μL of 10 mg/mL UCNPs mentioned above were added with vigorous stirring for 30 min. Next, 10 mL of distilled water was added dropwise to the above organic phase and the mixture was ultrasonicated for 20 min to be emulsified. The 12-h stirring of the emulsified solution was performed at room temperature for the evaporation of the organic solvent. The solution was then dialyzed for 24 h against distilled water to remove the residual organic solvent and impurities.

The NIR-responsive PEG detachment of iPUN was analyzed by DLS and ^{1}H-NMR. Typically, 1 mL of the aqueous solution with 0.5 mg/mL of iPUN was put into a vial and then irradiated with 980 nm NIR light (1 W/cm^2). After 5 min, the hydrodynamic diameter and zeta potential of the particles were determined by DLS at 20 °C applying Zetasizer Nano S. To study the change of iPUN under NIR irradiation, 20 mg of lyophilized iPUN sample was dissolved in 600 μL of $CDCl_3$. After NIR irradiation (1 W/cm^2, 1 cm^2 faculous region) for different time, iPUN containing solution was centrifuged, and the supernatant was collected for ^{1}H-NMR characterization. Similarly, the acid-responsive size and zeta potential change of iPUN was also analyzed by DLS. The preparation of TEM samples was made below: a drop of the solution containing UCNPs or iPUN was dripped on a carbon-coated copper grid (400-mesh) and absorbed off the excess solution from the edge of the grid by filter paper after 1 min (repeated for 3 times). The measurement of the mean diameters of particles was performed from 10 particles in the TEM micrographs.

Synthesis and Characterization of TPP-DOX (TDOX)

To be brief, 45 mg (0.10 mmol) of TPP was added to 10 mL of anhydrous *N*,*N*-dimethylformamide (DMF) in a 25 mL round-bottom flask and stirred to dissolve completely. Then, DCC (25 mg, 0.012 mmol) and NHS (14 mg, 0.12 mmol) were added into the above solution. After stirring for 3 h, the centrifugation of the mixture was conducted to eliminate dicyclohexylurea (DCU), and the collection of supernatant was conducted. Next, the purchased DOX (60 mg, 0.10 mmol) was desalted by using marginal excess of triethylamine. The activated TPP was then appended dropwise to the DOX solution. The solution was kept stirring for 12 h at room temperature in dark. Afterward, the crude product was obtained by precipitation in a great excessive amount of diethyl ether and centrifugation. Then, the precipitate was dissolved in chloroform and rinsed with saturated sodium chloride solution to remove other impurities from the product. The organic phase was then collected and dried in a vacuum. TDOX was characterized by FTIR (KBr pellet). Zetasizer Nano ZS90 (Malvern Instruments Company, UK) was adopted to perform Zeta potential analysis.

Preparation and *In vitro* TDOX Release of iPHM@UCNPs-TDOX (iPUTDN) Nanoparticles

To prepare iPUTDN, a similar route for the preparation of iPUN was exploited. Briefly, oleic acid-coated UCNPs were dissolved in cyclohexane. HTMP (10 mg), iPHT (4 mg), and TDOX (1, 2 or 5

https://doi.org/10.1007/s10118-022-2775-4

mg) were dissolved in chloroform. Firstly, the solutions were mixed, and distilled water was appended dropwise to the organic phase under vigorous stirring. After another 12 h stirring, the dialysis of the solution against water was conducted. iPUTDN nanoparticles were obtained by lyophilization.

$$\text{TDOX-loading content (\%)} = \frac{\text{Weight of loaded TDOX}}{\text{Weight of copolymers + Weight of loaded TDOX}} \times 100\% \quad (1)$$

$$\text{TDOX-loading efficiency (\%)} = \frac{\text{Weight of loaded TDOX}}{\text{Weight of feeding TDOX}} \times 100\% \quad (2)$$

To examine the TDOX release profile of iPUTDN under different conditions, four groups of samples were produced containing the same concentration of TDOX at 0.1 mg/mL. The conditions were set as solution pH at 7.4 or 5.0 and with or without NIR light irradiation. At predetermined time points, 3 mL of solution was collected from the vial containing 20 mL of solution for the measurement of TDOX absorbance at 480 nm, and 3 mL of fresh buffer was appended for keeping the volume in the vial. The calculation of the concentrations of TDOX was performed from a standard curve of TDOX absorbance at 480 nm.

Cell Culture and Cytotoxicity of Nanoparticles

DOX-resistant small-cell lung cancer H69AR cells were kindly given by Prof. Linglang Guo (Zhujiang Hospital, Southern Medical University). H69AR cells were used to examine the cell inhibition efficiency of iPUTDN. H69AR cells were cultured with RPMI supplemented with 20% FBS, 1.0×10^5 U/L penicillin (Sigma), and 100 mg/L streptomycin at 37 °C in 5 % CO_2. H69AR cells were seeded into a 96-well cell culture plate (8000 cells per well) and incubated at 37 °C with 5% CO_2. A fresh culture medium was employed to replace the growth medium after 24 h. Afterward, iPUTDN or control samples (free TDOX and DOX) were added into wells (sample size=6). The irradiation of cells was performed with NIR laser (980 nm, 2 W/cm^2, 30 s) at 2 h and 12 h, and cultured for another 24 h. CCK-8 assays were adopted to determine cytotoxicity. An ELISA plate reader was adopted to measure the absorbance of every well at a test wavelength of 450 nm. The cell growth suppression of samples was calculated as follows:

$$\text{Cell viability (\%)} = \frac{I_{\text{sample}} - I_{\text{blank}}}{I_{\text{control}} - I_{\text{blank}}} \times 100\% \quad (3)$$

where I_{sample} and I_{control} mean the intensity decided for cells handled with various samples and for control cells (untreated).

Cellular Uptake and Internalization Pathways of Nanoparticles

H69AR cells were seeded in confocal dishes at a density of 2×10^4 cells per well for 24 h at 37 °C in 5 % CO_2. Afterward, DOX, TDOX or iPUTDN with or without NIR irradiation (1 W/cm^2, 2 min, maintenance concentration of DOX or TDOX at 2 μg/mL) were performed with the cells in RPMI 1640 at 37 °C in 5% CO_2 for 2 h and 24 h, respectively. Later, the cells were washed with PBS buffer three times. Then, the cells were stained with 5 μg/mL Hoechst 33342 at 37 °C for 10 min, then washed with cold PBS for three times and instantly observed with CLSM. The fluorescent intensity was measured by ImageJ. For the internalization pathways study, the incubation of cells was performed with various inhibitors such as nocodazole (10 μg/mL), chlorpromazine hydrochloride (1 μg/mL), amiloride hydrochloride hydrate (50 μmol/L), and genistein (100 μmol/L) in serum-free RPMI 1640 medium for 30 min before incubation with the iPUTDN or iPUTDN+NIR for another 4 h. To avoid the effect of NIR irradiation on cells, iPUTDN was irradiated with NIR (1 W/cm^2, 2 min) in an aqueous solution before adding to the cells. Later, 4% paraformaldehyde was adopted to fix the cells for 10 min and then washed with PBS for three times. 5 μg/mL Hoechst 33342 was employed to stain the cells at 37 °C for 10 min, then washed with PBS for three times. Confocal images were obtained by excitation of the samples at 561 and 405 nm. The fluorescent intensity was measured by ImageJ.

Intracellular Drug Distribution of Nanoparticles

H69AR cells were seeded in culture dishes at an initial density of 1×10^4 cells. After 24 h, TDOX, iPUTDN with or without NIR irradiation (1 W/cm^2, 2 min, equivalent to 2 μg/mL of TDOX) were appended and incubated with cells for another 24 h. After the incubation, the cells were washed with PBS solution and a fresh medium was added. 100 nmol/L Green fluorescent Mitotracker was added to dishes and incubated at 37 °C for 30 min. The nuclei were fluorescently visualized by staining with 5 μg/mL of Hoechst 33342. The cells were observed with CLSM.

Mitochondrial Membrane Potential

JC-1 was employed to monitor the potential of the mitochondrial membrane. The probe will transform a monomer (red fluorescence) to a converged state (green fluorescence) in response to low mitochondrial membrane potential. Typically, H69AR cells were cultured in 6-well plates (2×10^4 cells/well) for 24 h, then incubated with TDOX or iPUTDN with or without NIR for 2 h. iPUTDN was irradiated with NIR (1 W/cm^2, 2 min) in an aqueous solution before adding to the cells. JC-1 (500 μL, 10 μg/mL) was adopted to stain the cells for another 20 min. After rinsing twice, the examination of the cells was performed with a microplate reader (Infinite 200 Pro, Tecan, Zürich, Switzerland).

Intracellular ATP Level Detection

H69AR cells were cultured with 6-well plates (2×10^4 cells per well) for 24 h at 37 °C, then incubated with TDOX and iPUTDN with or without NIR for 4 h. To avoid the effect of NIR irradiation on cells, iPUTDN was irradiated with NIR (1 W/cm^2, 2 min), in an aqueous solution before adding to the cells. The ATP assay kit was adopted to examine ATP levels, which were measured by a multi-mode microplate reader (Spark^{TM} 10M, Tecan, Zürich, Switzerland). The ATP levels were decided on basis of the ATP standard curve.

Establishment of the Subcutaneous Xenograft Mouse Model of DOX Resistant Small Cell Lung Tumor

Beijing WeiTongLiHua Animal Co., Ltd. provided female BALB/c nude mice (4–6 weeks, 13±2 g). The preparation of DOX resistant subcutaneous model of small cell lung cancer was performed according to the procedure below. 4% Chloral hydrate at a dosage of 10 mL/kg was intraperitoneally injected to anesthetize female BALB/c nude mice, followed by a subcutaneous injection of 1×10^7 H69AR cells. In the case of a palpable tumor at the position of the leg, the mice were subject to the experiments below. All the animal experiments were conducted by the guidelines approved by the Animal Care and Use Committee of CAS Key Laboratory for Biomedical Effects of Nanomaterials and Nanosafety.

https://doi.org/10.1007/s10118-022-2775-4

Biodistributions of iPUN-Cy5 and TDOX in Tumor-bearing Mice

EDC/NHS coupling reaction was employed to synthesize iPUN-Cy5. To be brief, Cy5-NHS (Lumiprobe, USA) was appended to iPUN nanoparticles (mass ratio=1:1000) and then stirred for about 12 h. The product was obtained by lyophilization post extensive dialysis against distilled water for 24 h. Free Cy5 (200 μL) and iPUN-Cy5 (Cy5 concentration, 1 μg/mL) were intravenously administrated (n=3). For NIR group, the tumor was exposed to NIR irradiation (1 W/cm^2) for 5 min after administration for 30 min, 4 h and 12 h. At the time points of 1 h, 6 h, 24 h post-injection, Lumina III *in vivo* imaging system ($\lambda_{Ex}/\lambda_{Em}$=640/680 nm) took the fluorescent images of the living mice. Then, the mice were sacrificed and the tumors were extracted to immunostaining with the anti-CD31 antibody and Alexa Fluor®488 secondary antibody. Finally, the distribution of iPUN-Cy5 penetration from blood vessels was visualized by CLSM and the penetration depth and the fluorescence intensity of iPUN-Cy5 were analyzed by ImageJ. Similarly, free TDOX and iPUTDN (TDOX concentration, 8 mg/kg) were administrated into mice (1 W/cm^2 NIR irradiation was performed for 5 min at tumor area 30 min after *i.v.* injection). At 24 h after injection, the sampling and imaging of heart, liver, spleen, lung, kidney and tumor were conducted by an *ex vivo* imaging system with excitation wavelength 465/640 nm and emission wavelength 580/680 nm.

In vivo Antitumor Effects in Tumor-bearing Mice

Ten days after inoculation of H69AR cells, the treatment was performed every other two days at a dose of 8 mg/kg for TDOX, lasting for three weeks (n=5 per group). The intravenous injection was performed through the tail vein. Later, the tumor area was exposed to NIR (980 nm, 1 W/cm^2, 10 min) at 1 and 12 h post-injection. The monitoring of body weight and the palpable tumor was performed every two days. After the treatments, all the mice were sacrificed and tumors were dissected and weighted. H&E staining was adopted to analyze histological sections of the main organs.

Hemolysis

Whole blood (1 mL) taken from BALB/c nude mice was placed into a 4 mL centrifuge tube with 2.5 μL of 2% heparin sodium, the slow shaking of the mixture was performed. Later, after adding the same volume of normal saline, 10-min centrifugation was performed at 1500 r/min. The supernatant was removed, and the dispersion of the precipitate was performed in 10 mL of normal saline. The 12-min centrifugation was conducted at 1500 r/min, and the red blood cell suspension (RCS) was obtained by repeating the same procedures three times. Later, (I) 0.8 mL of PBS as a negative control, (II) 0.8 mL of deionized water as a positive control, and (III) 0.8 mL of an aqueous dispersion of iPUN at various concentrations in a scope of 0–250 μg/mL were mixed with 0.2 mL of RBC suspension, respectively. The centrifugation of mixtures was performed (12000 r/min, 5 min) after a 1-h incubation at 37 °C, and optical density (OD value) was determined with the supernatants in a microplate reader at a wavelength of 541 nm.

Routine Blood Tests

After the treatments, the mice were anesthetized by injecting 4% chloral hydrate into the peritoneal cavity, and blood was collected by removing the eyeballs. Whole blood (100 μL) was added into the EP tubes with 1 mL of anticoagulation (1.5 mg/mL EDTA dipotassium salt dihydrate, Macklin, Shanghai, China) and the samples were examined with routine blood tests at Animal Laboratory Testing Center, Peking University Health Science Center.

H&E Staining and Ki-67 Immunohistochemistry Staining

At the end of treatments, the mice were sacrificed and mouse tumors were fixed in 4% paraformaldehyde at 4 °C overnight. The samples were cut as 5 μm slices and stained with H&E and Ki-67. The images were recorded by an inverted fluorescence microscope (Olympus IX73).

Statistics

Quantitative data are presented as mean±SD and analyzed by a two-tailed Student's t-test. P<0.05 was accepted as a statistically significant difference.

RESULTS AND DISCUSSION

Synthesis and Characterization of Nanoparticles

The synthesis of nanoparticles was performed according to a reported protocol.[32] The transmission electron microscopy (TEM) image implied that the UCNPs displays a uniform polyhedral morphology of ~30 nm in diameter (Fig. 1A). Upon illuminated with a 980 nm laser, UCNPs emitted multiple characteristic peaks at 340, 365, 450, 480, 580, 650, 690 and 720 nm, in which emission lights in the range of 320–380 nm were involved in the cleavage of Nbz bonds (Fig. 1D). According to the reported method, the light-sensitive copolymer HTMP and iRGD terminated copolymer iPHT were synthesized via Michael addition polymerization.[32] ^{1}H-NMR spectra characterization of copolymers was identical to the previous report,[32] indicative of the presence of PEG and PAE chains in HTMP, and the successful incorporation of Nbz bonds in HTMP and iRGD in iPHT, respectively (Fig. S1 in the electronic supplementary information, ESI). An ultrasonic-assisted solvent-substitution approach was adopted to prepare micellar nanoparticles.[34] The micellar nanoparticles without loading DOX (iPUNs) were firstly prepared (Table S1 in ESI), and TEM image of iPUNs shows a pomegranate-like morphology of ~130 nm in diameter (Fig. 1B). The oleic acid-capped UCNPs were encapsulated into the inner core of micelles due to strong hydrophobic interaction, and hydrophilic poly(ethylene glycol) (PEG) chains as the shell. Therefore, the composite iPUN nanoparticles can self-assemble in aqueous media to form stable core-shell type pomegranate-like nanoparticle structures. A pale grey corona existing around the clustered dark UCNPs nanocrystals connoted the successful preparation of the core-shell structural nanoparticle. Dynamic light scattering (DLS) measurements demonstrated a diameter decrement of iPUN from ~127 nm to ~106 nm upon NIR irradiation for 5 min (1 W/cm^2), corroborating the NIR induced dePEGylation of iPUN (Fig. 1C, Table S2 in ESI). Moreover, decay of the peak at ~5.25 ppm observed in ^{1}H-NMR spectra (Fig. 1E) suggested the degradation of the benzyl ester group of Nbz bonds in rPAE. The overlap between UV absorption bands of Nbz bonds and emission peaks of UCNPs suggests the possibility of UCNPs-mediated Nbz cleavage (Fig. 1D). In addition, the intensity of peaks decay at ~365 and ~480 nm in iPUN, compared with free UCNPs, which implied that the absorption of Nbz groups in light-sensitive amphiphilic

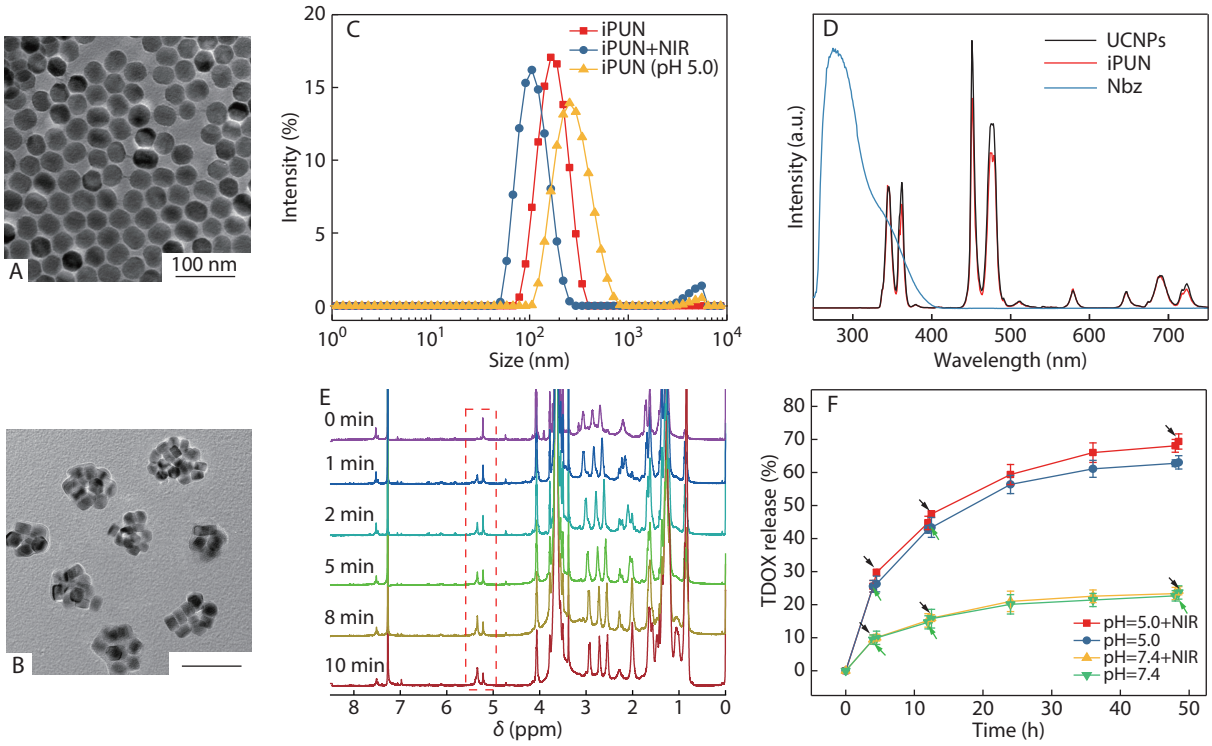

Fig. 1 Fabrication and characterization of UCNPs and iPUNs. (A) TEM image of UCNPs. Scale bar=100 nm. (B) TEM image of iPUN. Scale bar=100 nm. (C) The hydrodynamic diameter of iPUN, iPUN+NIR (1 W/cm^2, 5 min) and iPUN in 100 mmol/L pH 5.0 acetate buffer. (D) Upconversion emission spectra of free UCNP in hexane and iPUN in water under 980 nm excitation and UV-Vis absorbance spectra of Nbz in DMSO. (E) ^{1}H-NMR spectra of HTMP after irradiated by NIR (980 nm, 1 W/cm^2) over time. (F) The cumulative TDOX release profile of iPUTDN at different conditions (mean±SD, n=3). The green arrows indicate the time points of 980 nm laser on, and the black arrows mean laser off.

copolymers (Fig. 1D).

TDOX was synthesized according to the reference.[25] As shown in Fig. S2 (in ESI), TDOX exhibited a highly positive zeta potential of approximately +43 mV. Fourier transform infrared (FTIR) characterization of DOX and TDOX revealed the appearance of a band at 1652 cm^{-1} (C=O stretching of amide bond) in the TDOX spectrum, confirming the generation of the amide bond between DOX and TPP (Fig. S3 in ESI). TDOX was encapsulated into iPUN to construct iPUTDN with the weight ratio of TDOX/iPUN at 1/5. The cumulative TDOX release from iPUTDN under different conditions was examined (Fig. 1F). Approximately 24% of TDOX was slowly released in 48 h at pH 7.4, whereas ~63% of TDOX was discharged in 48 h at pH 5.0. TDOX release was accelerated upon NIR irradiation to ~70% at pH 5.0, partly because the PEG detachment favored the PAE core to contact the acidity milieu. In addition, DLS measurements of iPUTDN exhibit a size increase due to the protonation of PAE inducing the disassembly of nanoparticles (Fig. 1C, Table S2 in ESI). Taken together, NIR triggered PEG detachment of nanoparticles, which further accelerates the acid-sensitive dissociation of the nanoparticles.

Mitochondria Targeting and Cell Inhibition of Nanoparticles *In vitro*

Firstly, the cell uptake and intracellular distribution of TDOX were observed by confocal laser scanning microscopy (CLSM), using red emitted fluorescence of DOX at 630 nm when excited at 510 nm. After incubating H69AR cells with free DOX, TDOX, iPUTDNs with or without NIR at 2 h, the most intense red fluorescence was found in the TDOX and iPUTDN+NIR groups compared to other groups (Fig. 2A and Fig. S4 in ESI). After 24 h incubation, iPUTDN+NIR group retained the most intense fluorescence in four groups. Given that the H69AR cells are DOX resistant, it is reasonable to see the meager intracellular amount of free DOX at both time points. In stark contrast, iPUTDN plus NIR irradiation displayed a relatively slower but effective cell uptake because of the cascade behavior of PEG detachment and release of TDOX from particles.

Next, the endocytosis pathway of iPUTDN was investigated in the H69AR cells by CLSM. Chlorpromazine (CPZ) can restrain clathrin to suppress clathrin-dependent endocytosis.[35] According to Fig. S5 (in ESI), after incubating iPUTDN with the cells pretreated with CPZ (10 μmol/L), cellular uptake of DOX was declined compared with that of the control group. Similarly, when the cells were pretreated with amiloride and nocodazole,[36] cellular uptakes of DOX also decreased, indicating that clathrin-dependent endocytosis and macropinocytosis may involve in the cell uptake of iPUTDN. According to the outcomes, the uptake of PEGylated iPUTDN was energy-dependent endocytosis processes through clathrin-mediated and macropinocytosis pathways.

Mitochondrion targeting of DOX in the H69AR cell line under different conditions was examined by CLSM imaging. DOX shows a red fluorescence while mitochondria were labeled as green color. The co-localization of DOX with mitochondria displays merged yellow dots. As shown in Fig. 2(B),

https://doi.org/10.1007/s10118-022-2775-4

after incubating the cells with TDOX, iPUNTD, and iPUTDN + NIR for 24 h, iPUTDN + NIR group shows markedly more yellow dots than the other two groups and gives the highest Pearson's correlation coefficients from the analysis by ImageJ. In line with the results of cell uptake and changes in particle physicochemical properties, it verified that an effective translocation of DOX towards mitochondria was attributed to a cascade transform of nanoparticles, including the PEG peel-off by NIR, iRGD exposure promoting cell endocytosis of the particles, accelerated particle dissociation to release TDOX and TPP-inducing mitochondrial enrichment.

To acquire an insightful understanding of mitochondria-targeted chemotherapy, we explored the mitochondrial membrane potential and ATP level variation in H69AR cells. The test of mitochondrial membrane potential was performed by using the mitochondria permeable dye JC-1. The decline in the ratio of JC-1 emitted red/green fluorescence means mitochondrial depolarization.[37] H69AR cells incu-

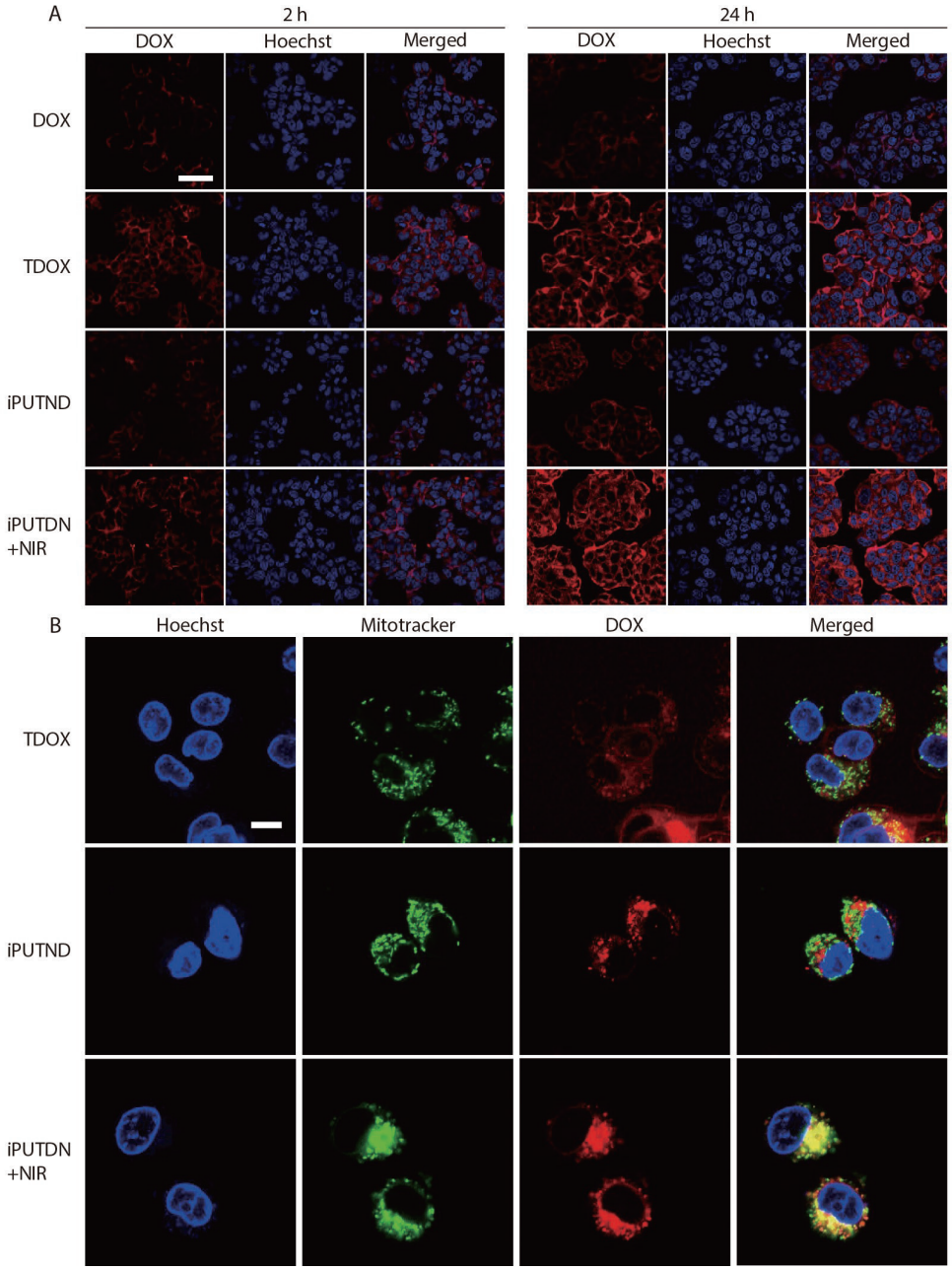

Fig. 2 Intracellular transport of iPUTDN in H69AR DOX resistance tumor cells. (A) Confocal microscopic images of H69AR cells incubated with DOX, TDOX and iPUTDN with or without NIR (980 nm, 1 W/cm^2, 2 min) for 2 h or 24 h. The nuclei were stained with Hoechst 33342 (blue). Scale bar=50 μm. (B) Colocalization images of TDOX (red) and mitochondria (green) in H69AR cells incubated with TDOX, iPUTDN or iPUTDN with NIR (980 nm, 1 W/cm^2, 2 min) for 24 h. Pearson's correlation is 0.775 (TDOX), 0.726 (iPUTDN), 0.898 (iPUTDN with NIR). Pearson's correlation coefficient for colocalization was obtained by colocalization analysis of NIS-Elements Viewer. Scale bar=10 μm.

https://doi.org/10.1007/s10118-022-2775-4

bated with TDOX, iPUTDN, or iPUTDN+NIR were stained with JC-1 for quantitative analyses by ImageJ from CLSM images. According to Figs. 3(A) and 3(B), the ratios of red/green fluorescence emitted by JC-1 were significantly declined in H69AR cells treated by TDOX, iPUTDN, or iPUTDN+NIR compared to the control sample. The result is consistent with their performance in cell uptake and mitochondria targeting. In the absence of NIR irradiation, the cascade transform of iPUTDN is inactivated, leading to a compromised function in depolarizing mitochondria membrane potential. In virtue of NIR, the activation of cascade DOX delivery by iPUTDN efficiently depolarized the mitochondrial membrane. As shown in Fig. 3(C), an evident decline in the intracellular ATP levels can be found in TDOX, iPUTDN, or iPUTDN+NIR groups. Mitochondrial membrane potentials are pivotal to sustaining ATP synthesis. Loss of mitochondrial membrane potentials incites a series of cell activities to induce apoptosis.[38] As the Pgp efflux pump is ATP-dependent, TDOX-induced depolarization of mitochondrial membrane potentials and subsequent decline of ATP levels might explain the suppression of Pgp-mediated drug efflux in H69AR cells. The effective cell endocytosis and damage of mitochondria by iPUTDNs in the presence of NIR light synergistically overcame the drug resistance by the cascade stimuli-responsive transformation.

In vitro cell inhibition efficacy of DOX, TDOX, iPUTDN, or iPUTDN plus NIR against H69AR cells was investigated by CCK-8 assay (Fig. 3D and Fig. S6 in ESI). The IC50 value of DOX in H69AR cells was 20.3 μg/mL, whereas the IC50 value of TDOX was reduced to 8.4 μg/mL. iPUTDN plus NIR irradiation exhibits a slightly higher cell inhibition ability (IC50=~7.5 μg/mL) in comparison to TDOX. The result implied that the cascade stimuli-responsive change of iPUTDN with the assistance of NIR ensured the rapid cell endocytosis and efficacious inhibition of drug efflux, which outperformed the other carriers.[39]

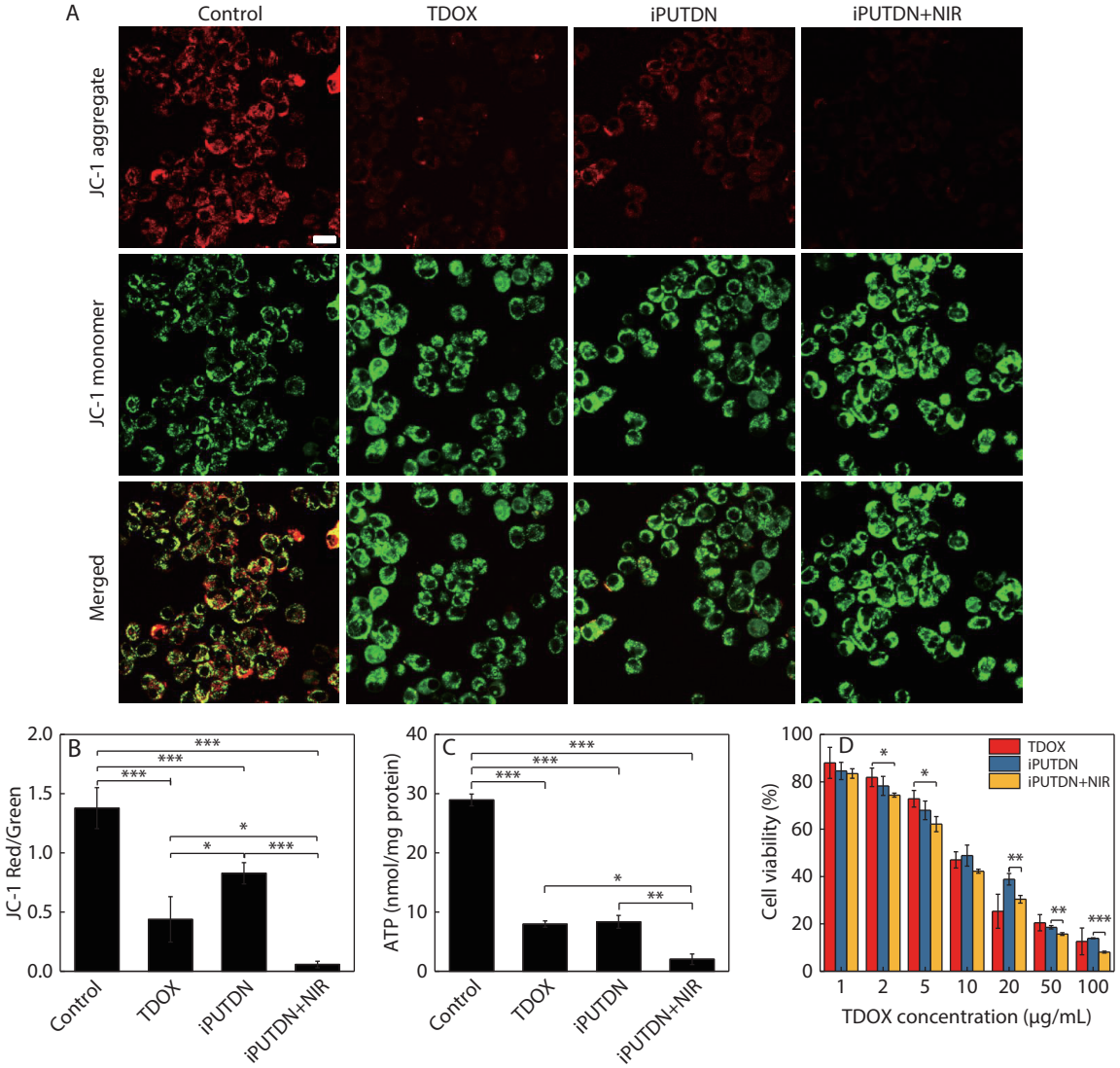

Fig. 3 The mechanism of iPUTDN to overcome DOX resistance in H69AR tumor cells. (A) Confocal images of mitochondrial membrane potential were examined by JC-1 as a probe. Scale bar=20 μm. (B) The JC-1 red/green fluorescence ratio in Fig. 3(A) is measured by ImageJ. (C) The effect of various samples on intracellular ATP was shown. The concentration of TDOX was maintained as 2 μg/mL. (D) Cell viability of free TDOX, iPUTDN and iPUTDN with NIR (980 nm, 2 W/cm^2, 30 s) in H69AR cells (mean±SD, n=6). *, P<0.05; **, P<0.01; ***, P<0.001.

https://doi.org/10.1007/s10118-022-2775-4

Biodistribution of Nanoparticles *In vivo*

To examine the distribution of nanoparticles *in vivo*, we established a BALB/c nude murine model bearing a subcutaneous H69AR tumor. Cy5 was modified onto iPUN or iPUTDN *via* EDC/NHS reaction between *N*-hydroxysuccinimide group on Cy5-NHS and amino groups on iPUN or iPUTDN. The fluorescent nanoparticles were conducive to being monitored *in vivo*. After intravenous injections of different samples, the live fluorescence of Cy5 in mice was monitored at 1, 6, and 24 h by Lumina III *in vivo* imaging system. According to Fig. 4(A), Cy5 fluorescence gradually elevated over time in mice injected with iPUN-Cy5. Upon NIR irradiation, iPUN-Cy5 exhibits a superior accumulation in tumors of mice by comparing with that of the no radiation group (Fig. S7A in ESI). Moreover, we next examined DOX distribution in mice by visualizing its *ex vivo* fluorescence in excised tissues of mice handled with TDOX, iPUTDN, iPUTDN + NIR after administration for 24 h. Similarly, DOX delivered by iPUTDN plus NIR shows more efficient tumor

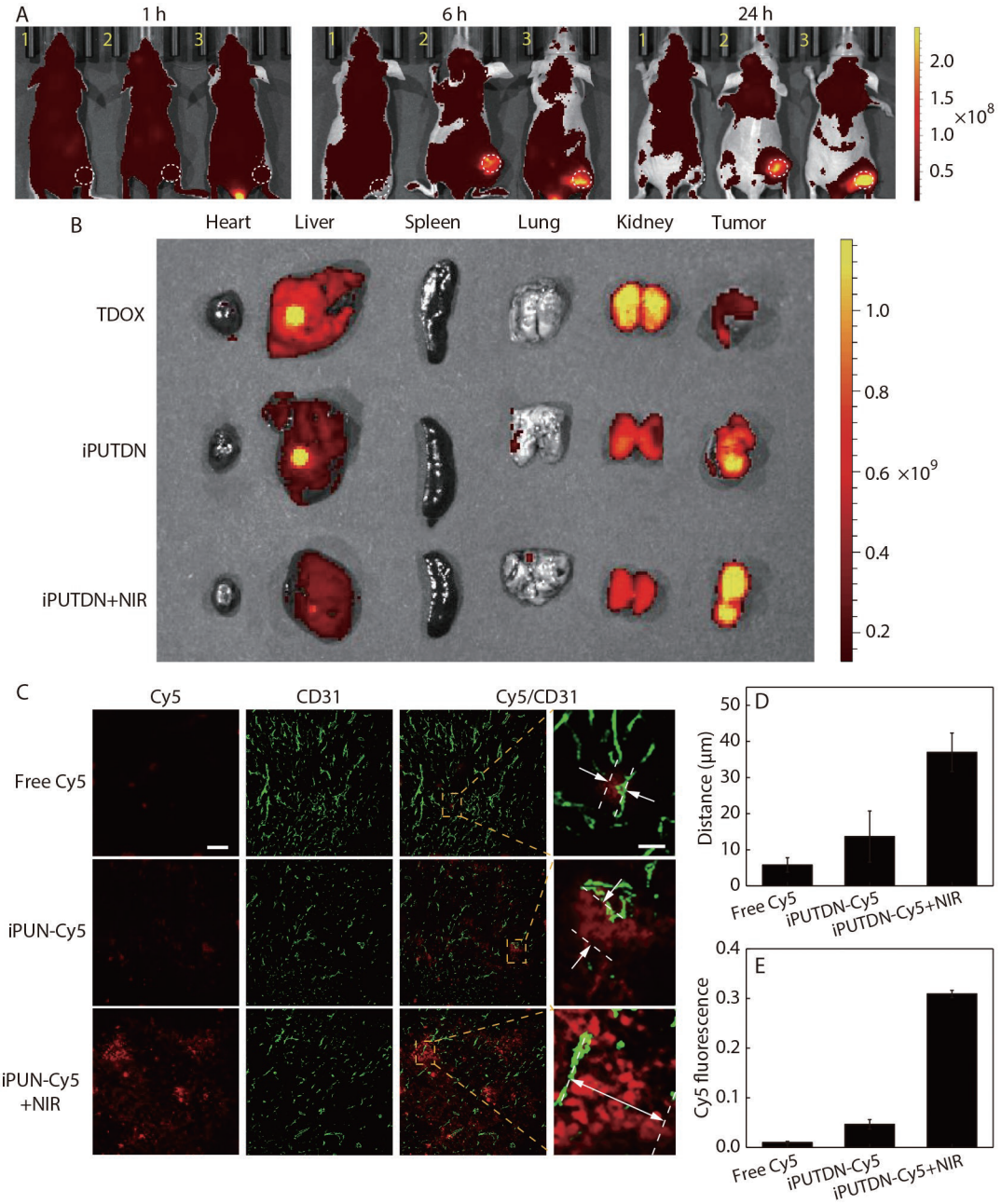

Fig. 4 Biodistribution of iPUN *in vivo*. (A) Fluorescence imaging of live mice upon 1. free Cy5; 2. iPUN-Cy5; 3. iPUN-Cy5 with NIR (1 W/cm^2, 5 min). The white circles emphasize the areas of tumors; (B) Fluorescence imaging of excised tumors and organs of mice upon free TDOX, iPUTDN, and iPUTDN with NIR (1 W/cm^2, 5 min); (C) Analysis of Cy5-labeled nanoparticles distribution in tumors. The immunostaining of tumor blood vessels was performed with CD31 antibody. Scale bar=50 μm. For magnified images. Scale bar=10 μm. (D) The mean distance between Cy5 labeled nanoparticles and the blood vessels from (C); (E) Cy5 fluorescence of CD31-stained tumor tissues was quantified by ImageJ (mean±SD, *n*=4).

https://doi.org/10.1007/s10118-022-2775-4

accumulation than the other two samples (Fig. 4B and Fig. S7B in ESI).

To examine the vascular penetration of nanoparticles, the immunostaining of tumor tissues at 24 h after injection was performed with fluorescently remarked CD31 antibody to visualize blood vessels. According to Fig. 4(C), the extravasation of considerably more Cy5-labeled nanoparticles was conducted from the tumor blood vessels by NIR than no NIR regulation because of NIR-caused activation of iRGD and downsizing of nanoparticles by NIR. There was even less Cy5 fluorescence around blood vessels in the free Cy5 group (Fig. 4E) because of the low cumulation of free Cy5 in tumors. Moreover, the average distance between nanoparticles and the tumor blood vessels was the longest in iPUN-Cy5/NIR group (Fig. 4D), suggesting improved penetration capability.

In vivo Antitumor Effects

The biocompatibility of the nanoparticles *in vivo* was investigated in the subcutaneous H69AR tumor-bearing BALB/c nude mice. The *i.v.* injection of iPUN at the highest dosage (250 μg/mL) did not cause hemolysis of the red blood cells (Fig. S8 in ESI). After administering the samples and NIR irradiation, mice's body weights kept similar between these groups for three weeks (Fig. 5A). There was no obvious variation in routine blood biochemical tests (Fig. S9 in ESI). These results attested that the administration of iPUTDN with or without NIR irradiation was biocompatible in mice. In the meantime, the

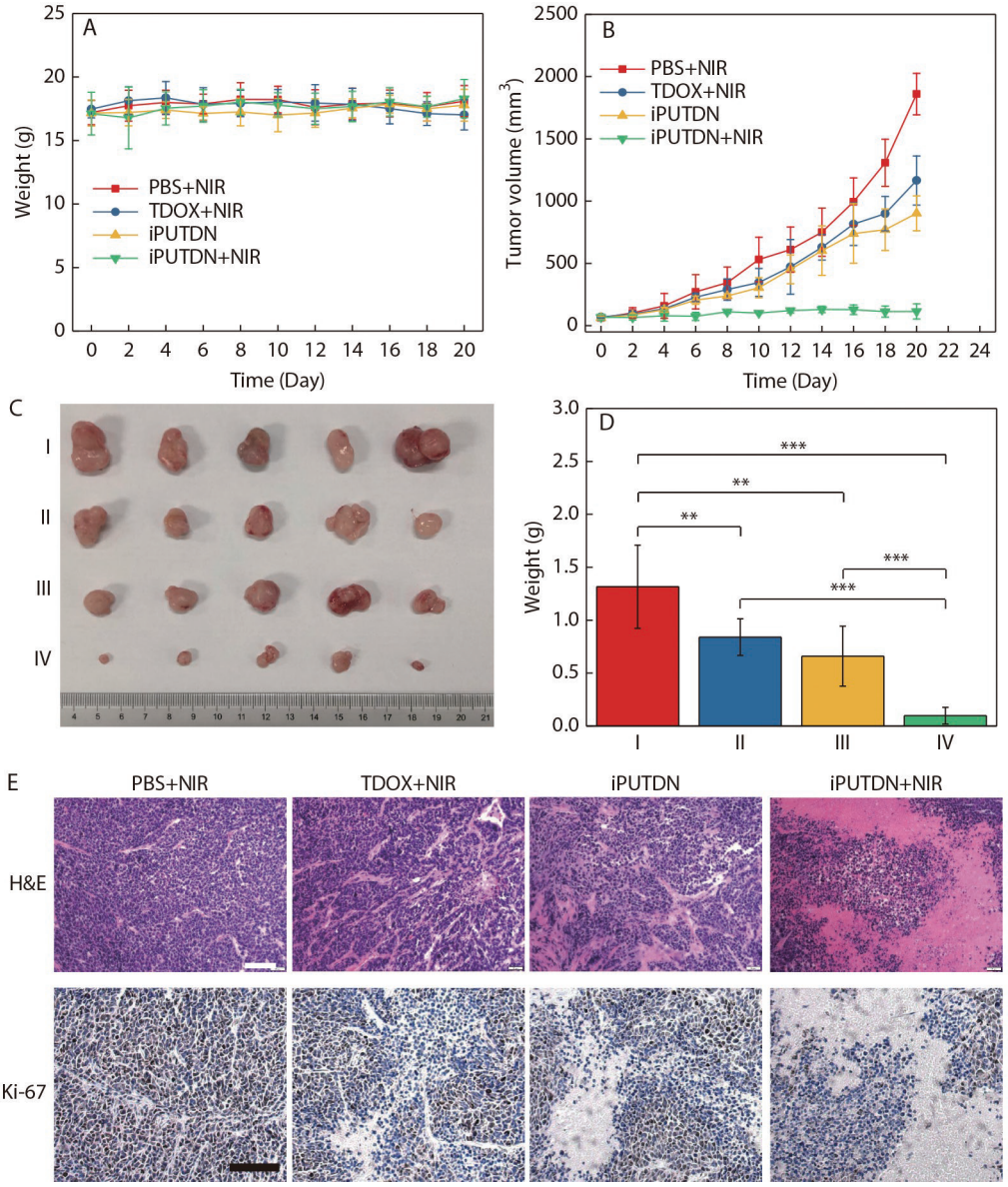

Fig. 5 Inhibitory effect of iPUTDN in DOX resistant H69AR tumor in BALB/c nude mice. (A) Average body weights of mice upon indicated treatments in three weeks (mean±SD, n=5). (B) Variations in tumor volumes during the treatment cycle (mean±SD, n=5). (C) Tumor dissection photographs from the mice through intravenous administration. I: PBS + NIR, II: TDOX + NIR, III: iPUTDN, IV: iPUTDN + NIR. (D) Average tumor weights in (C) (mean±SD, n=5). **, P<0.01; ***, P<0.001. (E) Representative pictures of H&E and Ki-67 staining of the excised tumors from each group after the treatments, respectively. Scale bar=20 μm.

https://doi.org/10.1007/s10118-022-2775-4

analyses for hematoxylin and eosin (H&E) staining of healthy organs after administration of iPUTDN revealed no severe adverse effects on the liver and kidney (Fig. S10 in ESI).

The examination of the *in vivo* anticancer therapeutic efficacy of the nanoparticles against a drug-resistant subcutaneous H69AR tumor in BALB/c nude mice was performed. By comparing with the controls, iPUTDN plus NIR irradiation potently restrained the tumor growth in mice for three weeks (Fig. 5B). The significant reduction in tumor weights after the treatments also proved the antitumor effects of iPUTDN with NIR irradiation (Figs. 5C and 5D). In addition, hematoxylin and eosin (H&E) staining of the tumor section at the end of the treatment indicated that the tumor cells exhibited less proliferation and the apparent propensity of apoptosis with the treatment of iPUTDN + NIR as compared to the other treatment groups (Fig. 5E). Similar results were found in the Ki-67 staining (Fig. 5E).

Subcellular organelle-targeted drug delivery has been reported as a promising way to improve disease diagnosis and therapy.[40] For lung cancer, one of the most aggressive malignant tumors, MDR is the major challenge leading to the current chemotherapy's failure. MDR results from various mechanisms associated with the abnormal mitochondrial activity. For example, MDR is caused by the overexpressed of drug efflux pumps, which require the involvement of mitochondrial ATP. Therefore, inhibiting the mitochondrial activities through targeted delivery of drugs to mitochondria would be an effective therapeutic approach to overcome drug resistance in chemotherapy.[41] However, the pathophysiological barriers impede the penetration of drugs into tumors, impairing the mitochondria-targeted drug accumulation.[42,43] Intelligent drug delivery nanosystems are recognized as promising tools to overcome pathophysiological barriers, and the development of effective nanosystems is in urgent demand.[44–46]

Numerous endogenous stimuli-responsive mitochondria-targeted nanosystems have been developed,[40–46] but the external stimuli-responsive nanosystems for mitochondrial-targeted drug delivery are less reported.[44–46] In this work, the NIR light-controlled PEGylation/dePEGylation strategy was developed to solve the PEG dilemma, which prolonged the circulation in the bloodstream and improved the targeted enrichment inside the tumor of iPUTDN. By exploiting their fluorescence upconverting ability, UCNPs can act as the inner light source by upconverting the extracorporeal NIR light to shorter-wavelength light, achieving the cleavage of HTMP copolymers. This feature allows us to develop the pH/NIR-dual responsive nano-drug carrier, thus realizing remote activation of the iPUTDN and cascade drug delivery upon NIR light. The present design seeks to circumvent the limitations of UV light, such as poor biological penetration and damage to tissue evoked by its high phototoxicity. Together, the *in vitro* and *in vivo* results indicated that the cascade nanomedicine targeted and penetrated deeply into the tumor tissue and delivered TPP-DOX to mitochondrial, effectively reversing drug resistance in lung cancer.

CONCLUSIONS

In summary, a cascade stimuli-responsive micellar nanoplatform has been developed for overcoming DOX resistance in small-cell lung cancer. In blood circulation, the PEGylated stealth nanoparticles could keep inert to elongate their circulation time, conducive to nanoparticle accumulation in tumor tissues. The embedded UCNPs effectively convert localized NIR to UV to break the photosensitive bond. As a result, removing PEG and exposing iRGD of nanoparticles enhance the tumor penetration and uptake efficacy by the tumor cells. Furthermore, through the integration of PAE-afforded lysosomal escape ability and the TPP-afforded mitochondria targeting, TDOX could efficiently accumulate in mitochondria. By TDOX-induced mitochondrial dysfunctions, intracellular ATP levels have dwindled. The activities of ATP-dependent Pgp pumps are inhibited and DOX efflux is interrupted, thereby enhancing the antitumor effects of DOX against DOX-resistant lung cancer. Overall, this study presents a promising strategy to combat DOX-resistant cancer.

NOTES

The authors declare no competing financial interest.

Electronic Supplementary Information

Electronic supplementary information (ESI) is available free of charge in the online version of this article at http://doi.org/10.1007/s10118-022-2775-4.

ACKNOWLEDGMENTS

This work was financially supported by the National Natural Science Foundation of China (Nos. 11875269 and 21574136), and the Beijing Natural Science Foundation (No. 7212212).

REFERENCES

1 Wang, H.; Gao, Z.; Liu, X.; Agarwal, P.; Zhao, S.; Conroy, D. W.; Ji, G.; Yu, J.; Jaroniec, C. P.; Liu, Z.; Lu, X.; Li, X.; He, X. Targeted production of reactive oxygen species in mitochondria to overcome cancer drug resistance. *Nat. Commun.* **2018**, *9*, 562.
2 Zeng, X.; Sun, J.; Li, S.; Shi, J.; Gao, H.; Sun Leong, W.; Wu, Y.; Li, M.; Liu, C.; Li, P.; Kong, J.; Wu, Y. Z.; Nie, G.; Fu, Y.; Zhang, G. Blood-triggered generation of platinum nanoparticle functions as an anti-cancer agent. *Nat. Commun.* **2020**, *11*, 567.
3 Jiao, D.; Yang, S. Overcoming resistance to drugs targeting KRAS(G12C) mutation. *The Innovation* **2020**, *1*, 100035.
4 Du, X.; Yang, B.; An, Q.; Assaraf, Y. G.; Cao, X.; Xia, J. Acquired resistance to third-generation EGFR-TKIs and emerging next-generation EGFR inhibitors. *The Innovation* **2021**, *2*, 100103.
5 Wang, H.; Liang, Y.; Yin, Y.; Zhang, J.; Su, W.; White, A. M.; Bin, J.; Xu, J.; Zhang, Y.; Stewart, S.; Lu, X.; He, X. Carbon nano-onion-mediated dual targeting of P-selectin and P-glycoprotein to overcome cancer drug resistance. *Nat. Commun.* **2021**, *12*, 312.
6 Christie, E. L.; Pattnaik, S.; Beach, J.; Copeland, A.; Rashoo, N.; Fereday, S.; Hendley, J.; Alsop, K.; Brady, S. L.; Lamb, G.; Pandey, A.; deFazio, A.; Thorne, H.; Bild, A.; Bowtell, D. D. L. Multiple ABCB1 transcriptional fusions in drug resistant high-grade serous ovarian and breast cancer. *Nat. Commun.* **2019**, *10*, 1295.
7 Johnson, Z. L.; Chen, J. ATP binding enables substrate release from multidrug resistance protein 1. *Cell* **2018**, *172*, 81–89.
8 Knudsen, J. G.; Hamilton, A.; Ramracheya, R.; Tarasov, A. I.; Brereton, M.; Haythorne, E.; Chibalina, M. V.; Spégel, P.; Mulder, H.;

Zhang, Q.; Ashcroft, F. M.; Adam, J.; Rorsman, P. Dysregulation of glucagon secretion by hyperglycemia-induced sodium-dependent reduction of ATP production. *Cell Metab.* **2019**, *29*, 430–442.
9 Zhang, J.; Song, X.; Xia, M.; Xue, Y.; Zhou, M.; Ruan, L.; Lu, H.; Chen, J.; Wang, D.; Chai, Z.; Hu, Y. The proximity of the G-quadruplex to hemin impacts the intrinsic DNAzyme activity in mitochondria. *Chem. Commun.* **2021**, *57*, 3038–3041.
10 Ruan, L.; Zhou, M.; Chen, J.; Huang, H.; Zhang, J.; Sun, H.; Chai, Z.; Hu, Y. Thermoresponsive drug delivery to mitochondria *in vivo*. *Chem. Commun.* **2019,** *55*, 14645-14648.
11 Wang, D.; Huang, H.; Zhou, M.; Lu, H.; Chen, J.; Chang, Y. T.; Gao, J.; Chai, Z.; Hu, Y. A thermoresponsive nanocarrier for mitochondria-targeted drug delivery. *Chem. Commun.* **2019**, *55*, 4051–4054.
12 Zheng, Y.; Ji, X.; Yu, B.; Ji, K.; Gallo, D.; Csizmadia, E.; Zhu, M.; Choudhury, M. R.; De La Cruz, L. K. C.; Chittavong, V.; Pan, Z.; Yuan, Z.; Otterbein, L. E.; Wang, B. Enrichment-triggered prodrug activation demonstrated through mitochondria-targeted delivery of doxorubicin and carbon monoxide. *Nat. Chem.* **2018**, *10*, 787–794.
13 Wolfram, J.; Ferrari, M. Clinical cancer nanomedicine. *Nano today* **2019**, *25*, 85–98.
14 Yamada, Y.; Satrialdi; Hibino, M.; Sasaki, D.; Abe, J.; Harashima, H. Power of mitochondrial drug delivery systems to produce innovative nanomedicines. *Adv. Drug Deliv. Rev.* **2020,** *154-155*, 187-209.
15 Wallace, K. B.; Sardão, V. A.; Oliveira, P. J. Mitochondrial determinants of doxorubicin-induced cardiomyopathy. *Circ. Res.* **2020**, *126*, 926–941.
16 Dong, X.; Sun, Y.; Li, Y.; Ma, X.; Zhang, S.; Yuan, Y.; Kohn, J.; Liu, C.; Qian, J. Synergistic combination of bioactive hydroxyapatite nanoparticles and the chemotherapeutic doxorubicin to overcome tumor multidrug resistance. *Small* **2021**, *17*, e2007672.
17 Keckesova, Z.; Donaher, J. L.; De Cock, J.; Freinkman, E.; Lingrell, S.; Bachovchin, D. A.; Bierie, B.; Tischler, V.; Noske, A.; Okondo, M. C.; Reinhardt, F.; Thiru, P.; Golub, T. R.; Vance, J. E.; Weinberg, R. A. LACTB is a tumour suppressor that modulates lipid metabolism and cell state. *Nature* **2017**, *543*, 681–686.
18 van den Bogert, C.; Holtrop, M.; Melis, T. E.; Roefsema, P. R.; Kroon, A. M. Different effects of oxytetracycline and doxycycline on mitochondrial protein synthesis in rat liver after long-term treatment. *Biochem. Pharmacol.* **1987**, *36*, 1555–1559.
19 Wang, M.; Ruan, L.; Zheng, T.; Wang, D.; Zhou, M.; Lu, H.; Gao, J.; Chen, J.; Hu, Y. A surface convertible nanoplatform with enhanced mitochondrial targeting for tumor photothermal therapy. *Colloid Surf. B* **2020**, *189*, 110854.
20 Liu, Y.; Li, H.; Xie, J.; Zhou, M.; Huang, H.; Lu, H.; Chai, Z.; Chen, J.; Hu, Y. Facile construction of mitochondria-targeting nanoparticles for enhanced phototherapeutic effects. *Biomater. Sci.* **2017**, *5*, 1022–1031.
21 Chen, M.; Wu, J.; Ning, P.; Wang, J.; Ma, Z.; Huang, L.; Plaza, G. R.; Shen, Y.; Xu, C.; Han, Y.; Lesniak, M. S.; Liu, Z.; Cheng, Y. Remote control of mechanical forces *via* mitochondrial-targeted magnetic nanospinners for efficient cancer treatment. *Small* **2020**, *16*, e1905424.
22 Krainz, T.; Gaschler, M. M.; Lim, C.; Sacher, J. R.; Stockwell, B. R.; Wipf, P. A Mitochondrial-targeted nitroxide is a potent inhibitor of ferroptosis. *ACS Cent. Sci.* **2016**, *2*, 653–659.
23 Huang, Y.; Li, Y. Drug delivery and reversal of MDR. *Mol. Pharmaceutics* **2014**, *11*, 2493–2494.
24 Cui, H.; Huan, M. L.; Ye, W. L.; Liu, D. Z.; Teng, Z. H.; Mei, Q. B.; Zhou, S. Y. Mitochondria and nucleus dual delivery system to overcome DOX resistance. *Mol. Pharmaceutics* **2017**, *14*, 746–756.
25 Bhatta, A.; Krishnamoorthy, G.; Marimuthu, N.; Dihingia, A.; Manna, P.; Biswal, H. T.; Das, M.; Krishnamoorthy, G. Chlorin e6 decorated doxorubicin encapsulated chitosan nanoparticles for photo-controlled cancer drug delivery. *Int. J. Biol. Macromol.* **2019**, *136*, 951–961.
26 Yang, R.; Wei, T.; Goldberg, H.; Wang, W.; Cullion, K.; Kohane, D. S. Getting drugs across biological barriers. *Adv. Mater.* **2017**, *29*, 1606596.
27 Gao, H.; Bi, Y.; Wang, X.; Wang, M.; Zhou, M.; Lu, H.; Gao, J.; Chen, J.; Hu, Y. Near-infrared guided thermal-responsive nanomedicine against orthotopic superficial bladder cancer. *ACS Appl. Mater. Inter.* **2017**, *3*, 3628–3634.
28 Jin, Q.; Deng, Y.; Chen, X.; Ji, J. Rational design of cancer nanomedicine for simultaneous stealth surface and enhanced cellular uptake. *ACS Nano* **2019**, *13*, 954–977.
29 Sun, Q.; Zhou, Z.; Qiu, N.; Shen, Y. Rational design of cancer nanomedicine: nanoproperty integration and synchronization. **2017,** *29*, 1606628.
30 Chen, B.; Dai, W.; He, B.; Zhang, H.; Wang, X.; Wang, Y.; Zhang, Q. Current multistage drug delivery systems based on the tumor microenvironment. *Theranostics* **2017**, *7*, 538–558.
31 Yang, Y.; Zhu, W.; Cheng, L.; Cai, R.; Yi, X.; He, J.; Pan, X.; Yang, L.; Yang, K.; Liu, Z.; Tan, W.; Chen, M. Tumor microenvironment (TME)-activatable circular aptamer-PEG as an effective hierarchical-targeting molecular medicine for photodynamic therapy. *Biomaterials* **2020**, *246*, 119971.
32 Zhou, M.; Huang, H.; Wang, D.; Lu, H.; Chen, J.; Chai, Z.; Yao, S. Q.; Hu, Y. Light-triggered PEGylation/dePEGylation of the nanocarriers for enhanced tumor penetration. *Nano Lett.* **2019**, *19*, 3671–3675.
33 Zhu, Y.; Chen, C.; Cao, Z.; Shen, S.; Li, L.; Li, D.; Wang, J.; Yang, X. On-demand PEGylation and dePEGylation of PLA-based nanocarriers via amphiphilic mPEG-TK-Ce6 for nanoenabled cancer chemotherapy. *Theranostics* **2019**, *9*, 8312–8320.
34 Deng, H.; Yang, W.; Zhou, Z.; Tian, R.; Lin, L.; Ma, Y.; Song, J.; Chen, X. Targeted scavenging of extracellular ROS relieves suppressive immunogenic cell death. *Nat. Commun.* **2020**, *11*, 4951.
35 Ingle, N. P.; Malone, B.; Reineke, T. M. Poly(glycoamidoamine)s: a broad class of carbohydrate-containing polycations for nucleic acid delivery. *Trends Biotechnol.* **2011**, *29*, 443–453.
36 Wang, J. L.; Tang, G. P.; Shen, J.; Hu, Q. L.; Xu, F. J.; Wang, Q. Q.; Li, Z. H.; Yang, W. T. A gene nanocomplex conjugated with monoclonal antibodies for targeted therapy of hepatocellular carcinoma. *Biomaterials* **2012**, *33*, 4597–4607.
37 Ren, J.; Sun, M.; Zhou, H.; Ajoolabady, A.; Zhou, Y.; Tao, J.; Sowers, J. R.; Zhang, Y. FUNDC1 interacts with FBXL2 to govern mitochondrial integrity and cardiac function through an IP3R3-dependent manner in obesity. *Sci. Adv.* **2020**, *6*, eabc8561.
38 Pai, J.; Hyun, S.; Hyun, J. Y.; Park, S. H.; Kim, W. J.; Bae, S. H.; Kim, N. K.; Yu, J.; Shin, I. Screening of pre-miRNA-155 binding peptides for apoptosis inducing activity using peptide microarrays. *J. Am. Chem. Soc.* **2016**, *138*, 857–867.
39 Zhou, M.; Zhang, X.; Xie, J.; Qi, R.; Lu, H.; Leporatti, S.; Chen, J.; Hu, Y. pH-sensitive poly(*β*-amino ester)s nanocarriers facilitate the inhibition of drug resistance in breast cancer cells. *Nanomaterials* **2018**, *8*, 952.
40 Zhen, W.; An, S.; Wang, S.; Hu, W.; Li, Y.; Jiang, X.; Li, J. Precise subcellular organelle targeting for boosting endogenous-stimuli-mediated tumor therapy. *Adv. Mater.* **2021**, *33*, e2101572.
41 Wang, H.; Shi, W.; Zeng, D.; Huang, Q.; Xie, J.; Wen, H.; Li, J.; Yu, X.; Qin, L.; Zhou, Y. pH-activated, mitochondria-targeted, and redox-responsive delivery of paclitaxel nanomicelles to overcome drug resistance and suppress metastasis in lung cancer. *J. Nanobiotechnol.* **2021**, *19*, 152.
42 Wu, M.; Zhang, H.; Tie, C.; Yan, C.; Deng, Z.; Wan, Q.; Liu, X.; Yan, F.;

Zheng, H. MR imaging tracking of inflammation-activatable engineered neutrophils for targeted therapy of surgically treated glioma. *Nat. Commun.* **2018**, *9*, 4777–4777.
43 Lamb, R.; Harrison, H.; Hulit, J.; Smith, D. L.; Lisanti, M. P.; Sotgia, F. Mitochondria as new therapeutic targets for eradicating cancer stem cells: quantitative proteomics and functional validation *via* MCT1/2 inhibition. *Oncotarget* **2014**, *5*, 11029–11037.
44 Liu, J. P.; Wang, T. T.; Wang, D. G.; Dong, A. J.; Li, Y. P.; Yu, H. J. Smart nanoparticles improve therapy for drug-resistant tumors by overcoming pathophysiological barriers. *Acta Pharmacol. Sin.* **2017**, *38*, 1–8.
45 Wang, J.; Zhou, M.; Chen, F.; Liu, X.; Gao, J.; Wang, W.; Wang, H.; Yu, H. Stimuli-sheddable nanomedicine overcoming pathophysiological barriers for potentiating immunotherapy of cancer. *J. Biomed. Nanotechnol.* **2021**, *17*, 1486–1509.
46 Huang, L.; Chen, F.; Lai, Y.; Xu, Z.; Yu, H. Engineering nanorobots for tumor-targeting drug delivery: from dynamic control to stimuli-responsive strategy. *ChemBioChem* **2021**, *22*, 3369–3380.

https://doi.org/10.1007/s10118-022-2775-4